1 Optical Design

Dark-field (DF) spectroscopy is the primary optical method used to study plasmonic nanostructures. The optical design employs the concept of reimaging spatial filters into the correct planes for efficient DF spectroscopy, leading to a compact design. Employing reimaging means that beams are not necessarily required to propagate exactly along the optical axis, minimising the number of long, empty beam lines, typically used for alignment. By reimaging the front and back focal planes of the objective, spatial and Fourier k-space filters are placed in the corresponding planes, ensuring optimum filtering performance and minimal aberration. A detailed schematic of the microscope platform and the surrounding optical bench layout, containing the specifications of all optics used, is found in Figure 1.

Both image and Fourier planes are set through careful placement of each set of lenses. The required minimum degrees of freedom for beam alignment are accounted for by mirrors placed in the focal and Fourier planes. Those in Fourier planes change the position of the beam without affecting it's shape, whereas those placed in focal planes only change the beam shape without shifting the position in the objective focus.[1] The position and shape of the beam are therefore independently adjustable, greatly simplifying beam alignment. This advantageous technique results in a high beam quality, and, as a direct result of the lack of long, iris-containing beam lines, a compact microscope.

A long working distance objective is required for imaging and spectroscopy. A bright-field (BF) long working distance IR objective (Olympus LMPlan 100× IR, 0.8 NA) is used to access wavelengths above 700 nm, for which the more convenient DF VIS objectives (Olympus LMPlan 100× BD) exhibit a sharp cutoff.[2] A DF illumination/collection configuration is necessary for spectrally studying scattered light from a nanostructure. Dark-field refers to the use of high-angle illumination, the reflections of which are filtered to collect only low-angle scattering from the focal plane. A large numerical aperture (NA) is required to properly study nanostructures in DF as it means light is collected across a large acceptance angle with a small focal length and large magnification. Since DF illumination is not supported on BF IR objectives, light needs to be brought in externally in a side-illumination geometry. A 3d-printed objective collar is used to hold a 1 mm diameter optical fibre ∼1–2 mm from the sample, outside of the objective collection angle, to which a cold white LED is fibre coupled. The fibre is fed through a breadboard hole in the top plate and sealed so as to preserve the environmental chamber integrity. The fibre outputs a broad cone of light which illuminates samples over a large area.

Use of a ultra-high brightness supercontinuum laser source (Fianium SC-400, 4 W, 480–1750 nm) enables single nanostructure spectroscopy with exposure times around 10–50 ms. The beam is expanded to fill the back aperture of the objective and apertured into a ring to mimic DF illumination using a DF disc stop. The inner diameter of the ring is set at 2 mm and the outer diameter is set by the back aperture of the objective, in this case 3 mm. This technique is a pseudo-DF method denoted supercontinuum dark-field (SDF). Reflective neutral density filters totalling ND 1.6 (2.5% transmission) are placed in the beam line to reduce the incident power on the sample. The majority of the incident power is lost at the DF stop. Further attenuation results from the 10:90 (R:T) beamsplitter used to relay the laser into the microscope. At this point the power is reduced to 1 mW, as measured on a bolometer (Coherent, inc.) behind the objective.[3] This prevents laser damage to samples. Whilst the power is seemingly low and comparable with high-brightness incoherent light sources, the focussing ability of the single mode laser results in an intense, diffraction-limited, white light focus not possible with incoherent sources. For an assumed broadband spot size around 1 µm the focal intensity is $\sim 10^8\,\mathrm{mW\,cm^{-2}}$.

The incident light is apertured and reimaged directly onto the back focal (Fourier) plane of the objective, as opposed to aperturing close to the objective back aperture. This prevents diffractive artefacts in the conjugate plane of the collected light. The ring aperture means that the focus is illuminated only at high-NA as with conventional DF spectroscopy. Scattered light is then filtered by a DF iris in the return beam path to remove any signal contribution from reflected, high-NA illumination. Reimaging allows both the DF iris and stop to be located away from the objective for convenient access and easy adjustment. Alternative designs using optics mounted at the objective back aperture do not benefit from having the stop and iris in conjugate planes and may require motorised irises if not accessible by hand. For this experiment a simple graduated dark-field iris is sufficient for external use to filter the collected light signal.

[1] Diagrams indicating the principles of beam alignment using reimaging are found in the appendices.
[2] A comparison of the two available 100× objectives is found in the appendices.
[3] Power characterisation found in the appendices.

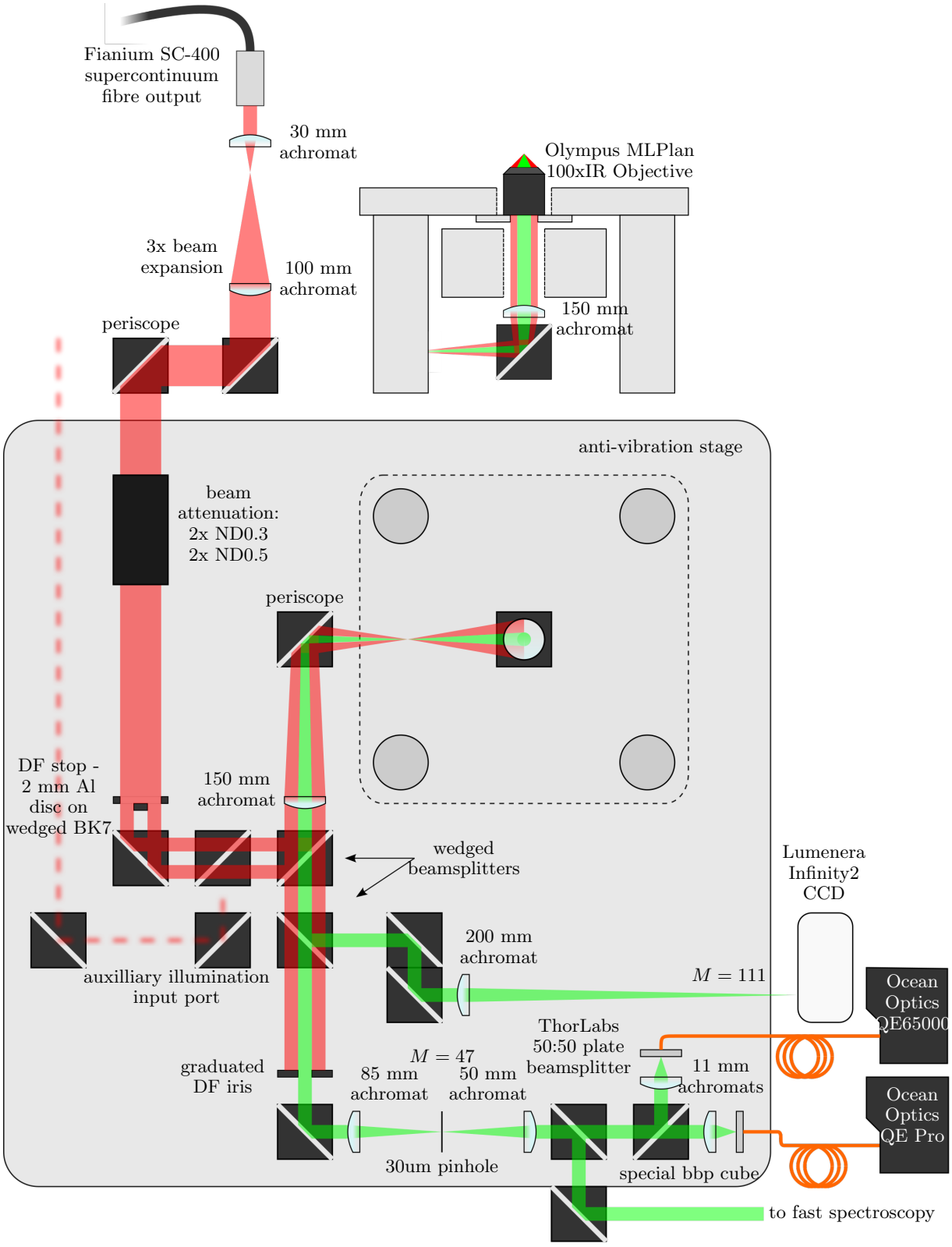

Figure 1: Diagram of the full optical layout and specification of the microscope. All optics are accounted for except for silver periscope mirrors, which transfer the beam between platforms of differing height.

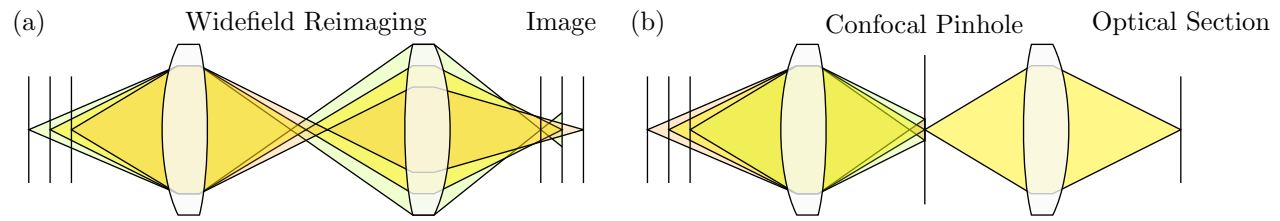

Figure 2: Diagram of optical sectioning in confocal microscopy. (a) Out of focus light from nearby reimaged focal planes leads to blur and a decrease of resolution in images. (b) Images spatially filtered in the focal plane by a confocal pinhole localise light from only a select volume that is sufficiently focussed to pass through the pinhole aperture.

Since incident power is not an issue, and in many cases requires significant attenuation, the microscope is optimised for efficient collection. The 10:90 beamsplitter used for laser input means only 10% of collected light is lost when returning back through the main microscope arm. Furthermore, all optics in the system are optimised for light between 500–1100 nm.[4] The angle-dependent Fresnel coefficients of the glass used in all optics components mean that *p*-polarised light is favoured during transmission throughout the microscope collection path.[5] A 90° turning periscope is placed after the first reimaging lens to reverse the linear polarisations of light so that the stronger *p*-polarisation component is orientated along the tip axis.

Subsequently, collected light is split into imaging and spectroscopy paths using a second (50:50) beamsplitter placed before the DF iris. CCD imaging is both used to align and characterise the laser focus and to centre samples onto the targeted laser illumination spot. Sample imaging uses light collected from the scattered white side-illumination LED light to produce DF images whereas the laser light is not DF-filtered in this path. Images are magnified 111×.[6] Light passing along the spectroscopy path is DF-filtered to remove any contributions to the scattering signal from reflected light. A graduated iris is used to remove the 2 mm outer-ring of the returning beam. The iris is placed in the image plane of the DF stop for the most accurate filtering and optimum performance. The two beamsplitters present before the DF iris are wedged to prevent ghost images, which transmit through the closed iris and create spectral artefacts. However, the 5 mm thickness of wedged beamsplitters means increased dispersion and the limited availability of broadband AR coatings results in reduced reflectance in the NIR. Additionally, the DF-filtering process only works to remove light reflected out at the same angle. Angled samples (such as the facets of tips) can reflect light into the low-NA collection, creating spectral artefacts. It is for this reason that the flat tip facets are even visible in a dark-field configuration.

1.1 Confocal Localisation of Spectra

Since the laser focusses to a diffraction-limited spot on the sample, spectra are collected from a small sampling volume. This single mode input forms the first component of confocal localisation. Further spectral localisation is achieved by confocally filtering the image plane after the DF iris using a 25 µm pinhole to collect light from only the central focal spot. Only light in focus on the pinhole may pass through it. By rejecting out of focus light the image becomes an optical section with a tighter depth of focus. The size of the pinhole sets both the lateral and axial width of the transmitted light and leads to both spatial masking and optical sectioning in the objective-sample plane, as shown in Figure 2. Spectra are therefore acquired from a localised sampling volume, as set by the location of the 47× demagnified pinhole image. The location of this spatial mask image in the objective focus is controlled by a mirror before the confocal filtering array. A slip-in disassembled webcam is used to image the Fourier plane before and after confocal filtering to check pinhole alignment. Since the depth of focus scales as M^2 (or NA^2) the placement of the pinhole along the beam path is not critical. Choice of pinhole diameter, however, is important.

[4] Broadband optimisation is achieved via exclusive use of Ag mirrors, Edmund Optics VIS-NIR AR coating on lenses, COMAR NIR and ThorLabs visible or visible-NIR coated beamsplitters.

[5] All beamsplitters have some degree of polarisation sensitivity due to Fresnel coefficients of the glass used. Reflectance can be a factor of 2 different between orthogonal linear polarisations. For comparison of glass reflectances and Fresnel coefficients see the appendix.

[6] Magnification is calculated by the ratio of focal lengths, $M = f_2/f_1$.

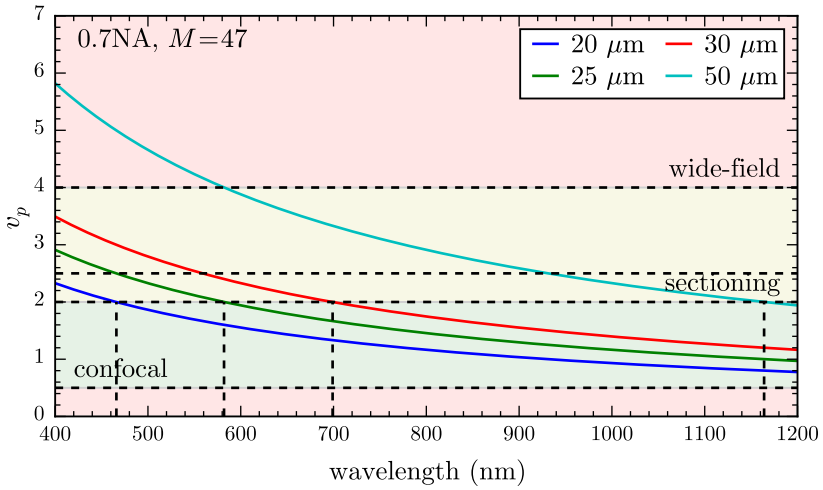

Figure 3: Optimum confocal pinhole size across the visible-NIR spectrum. A 25 µm pinhole is chosen for most experiments. Confocal performance is then achieved above 500 nm.

Confocal filtering not only improves image contrast but also improves upon the wide-field, diffraction-limited resolution by up to a factor of $\sqrt{2}$, depending on pinhole diameter, at the cost of image brightness [**webb1996confocal**, **murphy2002fundamentals**, **cox2004practical**, **hollricher2011high**]. This stems from the removal of higher diffraction orders by the pinhole. The resolution of a microscope is often quantified using the Rayleigh criterion - the distance from the maximum of the PSF (expected to be an Airy function) to the first minimum [**born1999principles**]. A decrease in the Rayleigh criterion of diffraction-limited resolution is expected in an epi-illumination geometry, going from $r_{\text{lateral}} = 0.61\lambda/NA$ down to $r_{\text{lateral}} = 0.44\lambda/NA$ at best. Decreasing the pinhole diameter therefore not only decreases the optical section thickness but also the minimum resolvable lateral distance to a certain extent.

For a realistic detector aperture the collection point spread function (PSF) is convoluted with its aperture function, D_p, giving an image PSF $I = |h_1|^2(|h_2|^2 * D_p)$ [**wilson1987size**]. The resulting resolution depends on a quantity v_p, the detector width, which can be related to the actual pinhole diameter, d_p, through [**wilson1987size**],

$$\frac{M}{NA} \geq \frac{\pi d_p}{v_p \lambda}. \tag{1}$$

The full-width half-maximum (FWHM) of the PSF retains the full, $\sqrt{2}$ improvement if $v_p \leq 0.5$, but this leads to a significant loss in brightness. An increased resolution is still in effect until $v_p \geq 4$, at which point the wide-field behaviour is recovered. Practically, $v_p \leq 2$ for optimal lateral resolution and $v_p \leq 4$ for optimal depth resolution. Optimising for $v_p = 2$ means that for a 0.7 NA, $M = 47$ system $d_p/\lambda \leq 43$, i.e. 21 µm at 500 nm and 47 µm at 1100 nm. A plot of v_p across the visible-NIR spectrum for a number of pinholes is shown in Figure 3, highlighting the relevant confocal regimes. For a given pinhole size that acts confocally in the visible, the intensity of some NIR wavelengths will be reduced since v_p drops below 1, however this loss is acceptable to maintain higher resolution in the visible region of the spectrum. A 25 µm pinhole size is determined to be optimal in this microscope based on this analysis and the range of available pinhole sizes.

Once filtered only the spectral content of the beam is of interest rather than the image so strict adherence to conjugate planes is no longer necessary. The beam is split 50:50 into two signals, with one going to the benchtop spectrometers and the other to a fast spectroscopy path.[7] The benchtop spectroscopy signal is further split into linear s and p polarisation components using a broadband polarising beamsplitter cube (Melles-Griot 300–1100 nm). Broadband polarisers (Thorlabs 500–1500 nm) oriented along the s and p axes are placed at the cube output ports to increase the extinction. Each polarised signal component is then finally focussed into multi-mode fibres, using short focal length (11 mm) lenses to achieve a spot size smaller than the fibre core. 100 µm fibre core

[7] The fast spectroscopy technique is developed and implemented but otherwise not used in any experiments in the current project. For this reason it's operation is omitted from this work.

is used instead of 50 µm to reduce laser speckle in spectra since the confocal pinhole diameter already localises the signal. The spectral signal from each of the fibres is recorded using TE-cooled, benchtop spectrometers (Ocean Optics QE65000 and QE Pro) with integration times between 10–50 ms. The sensitivity of the Si detectors in the spectrometers drops off beyond 900 nm, imposing a limit to detectable signals of around 1100 nm. The supercontinuum laser imposes a 480 nm spectral cut-on, resulting in an overall effective measurement window of 500–1100 nm.

Measured spectra are background-subtracted, to remove dark counts, and referenced to the spectral density of the supercontinuum illumination as transmitted through the microscope optics. Use of the intense supercontinuum source means low integration times below 20 ms are sufficient to near saturate the spectrometer for a high quality signal to noise. The high brightness of the supercontinuum laser at these exposures also means that the relative intensity contribution from external light sources is negligible. The coherence of the supercontinuum laser means that conventional referencing using scatter from a white diffuser to map the illumination spectral density is not possible. Instead, reflections from thin, reflective substrates attached underneath the piezo-mounted tip mount are used as a reference. Different substrates are used depending on the sample. For metallic samples the substrate is matched to the metal so only structural spectral features are observed. Otherwise either a Ag mirror or glass slide are sufficient for referencing as they provide relatively flat reflectances across the visible-NIR spectrum. The DF iris is kept fully open during reference acquisition to ensure the full spectral content of the incident beam is measured and to avoid introducing referencing artefacts. As optics are very rarely broadband between 500–1100 nm, all non-essential pathways are closed when acquiring spectra to prevent artefacts. Back reflections off lenses are found to superimpose a weak duplicate of the illumination spectrum onto spectra since the reflections are translated in k-space and are therefore not completely filtered by the DF iris.

1.2 Characterisation of Microscope Performance

During most experiments the power incident on samples is kept below 1 mW corresponding to a focal intensity of $\sim 10^8$ mW cm^{-2}. This is used to maintain sufficient signal quality whilst preventing damage or destructive changes to nanoscale Au samples (typically 50 nm Au coatings). Beam profiling is used to characterise beam propagation in the microscope and determine its ability to collect DF spectra. Profiling is carried out using focal scans of both light reflected from a Ag mirror and light scattered from an 80 nm AuNP, measured simultaneously on a CCD and a spectrometer. The CCD is used to laterally profile the beam through the focus while the spectrometer characterises the confocal profile and spectral distribution of the light. Both the illumination and collection pathways are profiled. The illumination pathway is profiled using the DF-filtered supercontinuum beam while one of the collection fibres is removed from its spectrometer and coupled to a 532 nm single mode laser in order to profile the collection pathway.

Figure 4 shows both the lateral focal spot on the CCD and relevant cross sections along the optical and focal axes for both the illumination and collection optics, along with depth-profiling using broadband-integrated spectra. Figure 4a shows the beam structure in the focus. The single mode fibre output exhibits the characteristic Airy profile expected of a Gaussian beam while the ring aperture of the supercontinuum beam leads to more power concentrated in the outer rings of the focal pattern (Figure 4b). The measured FWHM of the collection beam is (460 ± 20) nm with a beam waist (1/e width) of (540 ± 20) nm. The 47× demagnified image of the 25 µm pinhole is expected to be 530 nm. The focal radius of a single mode Gaussian beam (the beam waist) is given by $w_0 = \lambda/\pi NA$, which results in a collection NA of 0.62 ± 0.02. Measurement of a Rayleigh criterion length of (530 ± 20) nm indicates the beam is focussed through 0.61 ± 0.02 NA. Uncertainties on these calculations of the NA are small since the 532 nm wavelength is well known. Both calculations of the NA only partially agree due to beam focussing at the diffraction limit and both show a collection half-angle of $(38.0 \pm 0.5)°$. The axial cross section of beams (Figure 4c) shows the focussing of the high angle (0.64–0.8 NA, 40–53° incident angle) supercontinuum ring. The boundary between incident and collection beams is measured to be around 0.62 in both beam angle and spot size measurements since the DF iris diameter and the DF stop diameter are both set to 2 mm. The axial beam profile, however, measures the angle of light from the focus to below $(21 \pm 1)°$ (0.35 NA). This is likely caused by observation error due to the low intensities at high angles. After confocally filtering the depth of focus, as measured on the CCD beam profile, is on average 4 µm across the supercontinuum wavelength range (Figure 4d). This could potentially be improved by confocally filtering the supercontinuum input to become similar to a true confocal microscopes. In this case focal depths as low as 0.8 µm could be expected

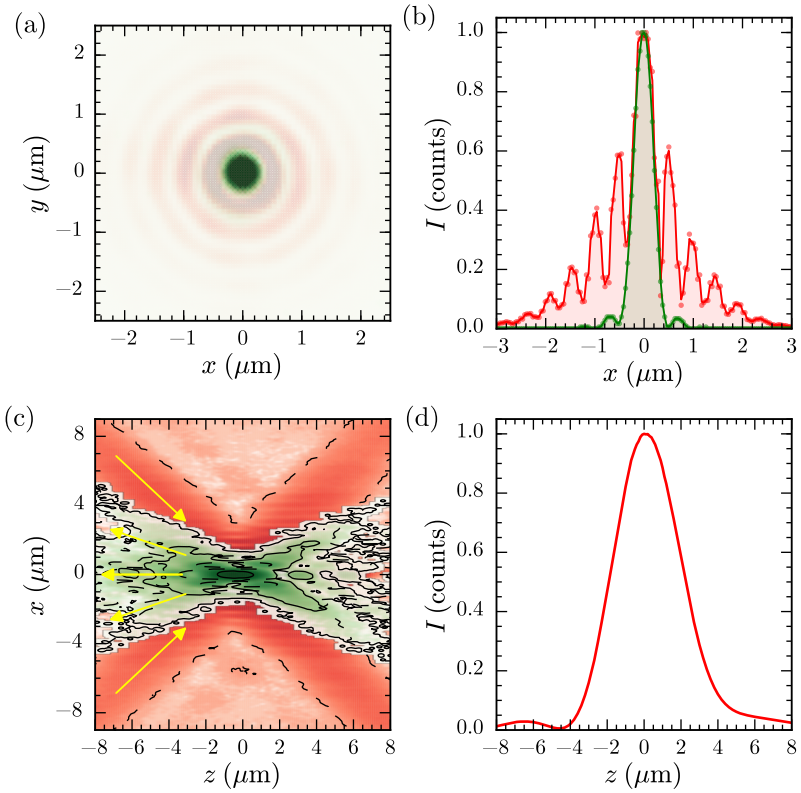

Figure 4: Beam profiling of dark-field filtered supercontinuum illumination (red) and scattering collection (green) beam lines. Supercontinuum laser light is reflected back from a Ag mirror in the objective focus to characterise the illumination pathway. The spectroscopy pathway is characterised by coupling a 532 nm laser into a single mode fibre and passing it through the collection optics with the DF-iris closed to 2 mm. The stated axial distance z is twice the displacement of the mirror to account for reflections to the focal plane. Lateral distances are calculated using the CCD array size and pixel dimensions. (a) Lateral beam profile of the illumination and collection focusses as measured on the CCD. (b) Intensity cross sections through the lateral beam profiles of the illumination and collection. (c) Axial cross section through the focus of illumination and collection beams. (d) Normalised summation of spectrometer counts of confocally localised supercontinuum light passing through the collection optics.

[**murphy2002fundamentals**]. For most cases it is not necessary since samples are suspended nanostructures and depth profiling is not necessary.

Figure 5 shows the individual wavelength components that make up the integrated spectral signal in Figure 4d. As expected the depth of focus increases with wavelength. The depth varies from (2.8 ± 0.1) µm at $\lambda = 500$ nm to (6.4 ± 0.1) µm at $\lambda = 1100$ nm. The chromatic structure of the beam is non-linear and shows that the colour maxima for $\lambda < 550$ nm and $\lambda > 800$ nm occur slightly offset from the pinhole position. Overall this does not detract much from the measured spectra since intensity differences in the chosen focal plane are normalised with the reference spectrum.

Lateral localisation is more important to consider than axial sectioning. Scattered light from a sub-wavelength size nanoparticle provides a point source from which the PSF can be measured across a small, resonant bandwidth. By (raster-) scanning a strongly-scattering metallic nanoparticle (MNP) under the beam its point scattering response is convoluted with the beam structure in the focus. The size of the confocal pinhole determines how much of this beam structure is laterally filtered prior to spectroscopy and thus, by measuring the scattering spectra, the actual PSF, as seen by the spectrometers, can be mapped across a broad range of wavelengths. It is this function that determines the specific locations from which spectra are collected and becomes particularly important when attempting to measure localised scattering from an extended nanostructure.

Figure 6 shows scattering profiles extracted from AuNP scans, demonstrating the effective spectral PSF for a

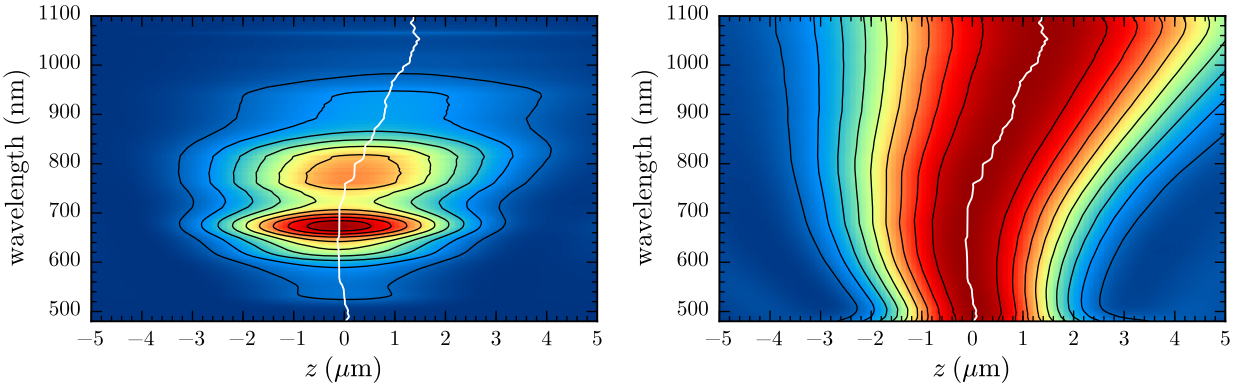

Figure 5: Axial chromatic aberration at each wavelength through the objective focus. The image is formed from spectra of the *s*-polarised component of a reflection from a Ag mirror scanned through the focus. An intensity plot normalised for each wavelength is shown to determine depth of focus. The white indicates the position of maximum signal along the optical axis for each wavelength and shows the distinctive bowing curve of chromatic aberration.

range of pinhole diameters. 80 nm AuNPs on glass resonantly scatter at 550 nm due to excitation of the dipolar localised surface plasmon (LSP). A single AuNP was chosen on which multiple scans were performed, changing and realigning the confocal pinhole in between each scan. Wavelength slices at the AuNP surface plasmon resonance (SPR) (Figure 6a–c) show the lateral effective PSF. Without a pinhole in place the spectral PSF is a convolution of the focal beam profile shown in Figure 4a. The spectrometer sees the scattering from all the concentric rings in the focus so localisation of spectral features would only be somewhat possible. Decreasing the pinhole diameter filters scattering from the focus and removes the contributions to spectra from the outer rings until spectra can only be acquired from the central spot. This guarantees localisation of observed spectral features to a finite-sized region. The FWHM of the scattering signals on resonance are (250 ± 25) nm with any pinhole in place and (300 ± 25) nm without a pinhole. The FWHM at 900 nm for the case of the 25 µm pinhole is 410 nm for reference. Due to the single AuNP being the only source of scattering in each of the scans the measured spectra is the same for all pinholes (Figure 6e).

Fitting the centroid at every wavelength in the spectral data cube identifies lateral chromatic aberration in the microscope. This is an important parameter to consider when using hyperspectral imaging or when acquiring spectra. For example, if the chromatic aberration is systematic and fitted then a correction offset can be added to hyperspectral data cubes at each wavelength. Spectra from each pixel can then be further recombined into regular RGB images by integrating the spectra at each pixel with RGB pixel spectra.

Figure 7 shows the centroids of the PSFs across the SPR band for each pinhole diameter. Scattering centroids are extracted from each wavelength slice using discrete image moment analysis,

$$M_{ij} = \sum_x \sum_y x^i y^j I(x, y), \tag{2}$$

where i, j denote the moments of the x, y axes.[8] The position of maximum scattering is then given by,

$$(\bar{x}, \bar{y}) = \left(\frac{M_{10}}{M_{00}}, \frac{M_{01}}{M_{00}} \right). \tag{3}$$

Displacements are scaled relative to the centroid position on resonance where the signal is highest. The centroid position drifts almost linearly by 80 nm in the x-direction and 80 nm in the y-direction. Since the pinhole only filters the outer rings of the PSF there is very little difference in the centroid positions between pinholes. As the

[8] Note that the discrete image moments are based on the continuous moment theorem with moments given by

$$M_{ij} = \int_{-\infty}^{\infty} \int_{-\infty}^{\infty} x^i y^j f(x, y) dx dy.$$

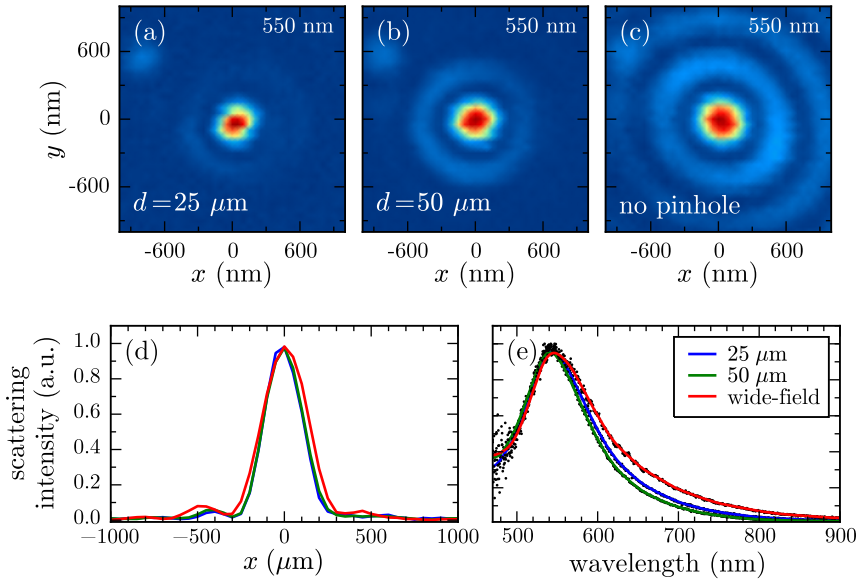

Figure 6: Hyperspectral scans of AuNPs used to characterise the lateral PSF with different confocal pinhole diameters. (a-c) Wavelength slices of AuNP scans on resonance using 25 µm and 50 µm diameter pinholes and finally no pinhole, respectively. (d) The extracted PSF from line profiles across the images (a-c). (e) Spectra of AuNPs imaged. Localisation is observed with reduced pinhole diameter as the concentric illumination rings are cut.

range of centroid displacement in each direction is well below the diffraction limit and corresponds to only a few pixels offset in each image, the aberrations are not considered to negatively impact spectroscopy.

To summarise, a microscope platform has been designed to accommodate various sample geometries, specifically AFM tips. Single nanostructure spectroscopy is enabled by utilising an ultra-high brightness supercontinuum laser in a dark-field optical geometry and capable of measuring spectra between 500–1100 nm with short exposures, as low as 10 ms. Beam profiling clearly shows that the supercontinuum dark-field technique works as expected and that spectra are collected from a small volume in the objective focus due to confocal localisation.

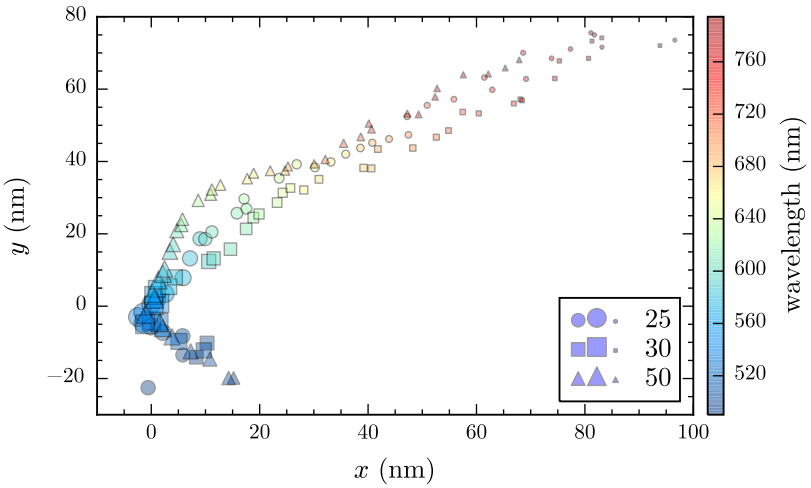

Figure 7: Measurements of lateral chromatic aberration across the plasmon resonance scattering bandwidth from hyperspectral images of AuNP. The central position of the scattering centroid is extracted from images at each wavelength. Changes in centroid position with wavelength signify chromatic aberration.